Experimental Bi-axial tensile tests of spinal meningeal tissues and constitutive models comparison

Yannick Tillier, Morgane Evin, Patrice Sudres, Pascal Weber, Yves Godio-Raboutet, Pierre-Jean Arnoux, Eric Wagnac, Yvan Petit

Journal : Acta BioMaterialia

TITLE:

Experimental Bi-axial Tensile Tests of Spinal Meningeal Tissues and Constitutive Models Comparison

Short title: Biaxial Tensile Tests of Meningeal Tissues

AUTHORS:

Morgane Evin[a,b] PhD, Patrice Sudres[a,b] PhD, Pascal Weber[e] MS, Yves Godio-Raboutet [a,b] PhD, Pierre-Jean Arnoux[a,b] PhD, Eric Wagnac[b,c,d] PhD, Yvan Petit[b,c,d] PhD, Yannick Tillier[f] PhD

AFFILIATIONS:

(a) Aix-Marseille Univ, Univ Gustave Eiffel, LBA, Marseille, France

(b) iLab-Spine - Laboratoire international en imagerie et biomécanique du Rachis, Marseille, France

(c) Department of Mechanical Engineering, École de Technologie Supérieure, 1100 Notre-Dame Street West, Montréal, Québec H3C 1K3, Canada

(d) Research Center, Hôpital du Sacré-Coeur de Montréal, 5400 Gouin blvd, Montréal H4J 1C5, Québec, Canada

(e) Institut de Neurosciences de la Timone, Marseille, France

(f) MINES ParisTech, Université PSL, Centre de Mise en Forme des Matériaux (CEMEF), UMR CNRS, 06904 Sophia Antipolis, France

Word count not including abstract, references, tables and figure legends: 5802

Tables and figures count: 11

Authors' emails: morgane.evin@univ-eiffel.fr ,

Corresponding author address:

Morgane Evin
iLab Spine - Laboratoire de Biomécanique Appliquée
UMRT24 Université Gustave Eiffel - Aix Marseille Université
Faculté de Médecine secteur-Nord
51 Bd. P. Dramard 13015 Marseille
Telephone number: (33)+4.91.65.87.58

ABSTRACT:

Introduction: This study aims at identifying mechanical characteristics under bi-axial loading conditions of extracted swine *pia mater* (PM) and *dura* and arachnoid complex (DAC).

Methods: 59 porcine spinal samples have been tested on a bi-axial experimental device with a pre-load of 0.01 N and a displacement rate of 0.05 $mm.s^{-1}$. Post-processing analysis included an elastic modulus, as well as constitutive model identification for Ogden model, reduced Gasser Ogden Holzapfel (GOH) model, anisotropic GOH model, transverse isotropic and anisotropic Gasser models as well as a Mooney-Rivlin model including fiber strengthening for PM. Additionally, micro-structure of the tissue was investigated using a bi-photon microscopy.

Results: Linear elastic moduli of 108±40 MPa were found for DAC longitudinal direction, 53±32 MPa for DAC circumferential direction, with a significant difference between directions ($p<0.001$). PM presented significantly higher longitudinal than circumferential elastic moduli (26±13 MPa vs 13±9 MPa, $p<0.001$). Transversely isotropic and anisotropic Gasser models were the most suited models for DAC ($r^2=0.99$ and RMSE:0.4 and 0.3 MPa) and PM ($r^2=1$ and RMSE:0.06 and 0.07 MPa) modelling.

Conclusion: This work provides reference values for further quasi-static bi-axial studies, and is the first for PM. Collagen structures observed by two photon microscopy confirmed the use of anisotropic Gasser model for PM and the existence of fenestration. The results from anisotropic Gasser model analysis depicted the best fit to experimental data as per this protocol. Further investigations are required to allow the use of meningeal tissue mechanical behaviour in finite element modelling with respect to physiological applications.

Keywords: bi-axial testing, meningeal tissue, *pia and dura mater*.

1. Introduction

The required understanding of physiopathology mechanisms involving meningeal tissue has already been investigated. Interest in *dura mater* mechanical behaviour has arisen by the post-subdural and epidural anesthesia-puncture headaches as well as in Chiari malformation [1]. The *dura mater* integrity contributes to cerebro-spinal fluid (CSF) resorption and to the balance of intra-cranial pressure in human [2]. The mechanical physiological strain associated with daily cranial volume expansion on *dura mater* growth has been quantified [3].

Additionally, *pia mater* (PM) and arachnoid mater (Figure 1-A) material properties have been reported to change global mechanical behaviour of the spinal cord [4]. Finite element modelling, initially addressing traumatic events, more recently included fluid structure interaction modelling of CSF to simulate physiology [5,6]. Such modelling requires specific material properties. In addition, prosthetic biomaterial scaffold engineering requires a comprehensive understanding of the meningeal tissues structure and material properties [7]. However, little is known on the mechanical properties of this meningeal tissue. A link between meningeal tissues' micro-structure and mechanical properties under physiological conditions remains unclear.

1.1. Meningeal micro-structure

The characterization of the micro-structure and collagen fibers of the meningeal tissues requires specific imaging techniques, including histology [8], two photon microscopy or scanning electron microscopy stereo images [8]. Few studies address the relation between structure composition and mechanical properties of meningeal tissues. The elastic modulus of porcine *dura mater* has been shown to be affected by the protein content in the cranial region according to its locations using immunoblot [9]. Micro-structure of the porcine dura mater is reported to be relatively similar to human *dura mater* [10].

At its cranial location, human *dura mater* was shown to be divided into three layers with different fiber arrangements and thicknesses:

- a bone surface layer of 2 µm thick (outermost layer) composed of fibroblast, collagen and elastin fibers. The outer part is a structure in which the collagen fibers are unstructured while the collagen fibers are parallel to each other in the inner part,
- a fibrous *dura* layer divided into three layers with their own arrangement. The external layer has one direction of collagen fibers, the vascular interlayer has holes and interstitial compartments and the internal layer has collagen fibers structured in bundles transversally oriented like the upper one,
- an arachnoid layer with unstructured collagen bundles [2].

The arachnoid layer in the subarachnoid canal has been described as an inner layer of *dura mater* [11] with trabeculae inserted in the PM and cells similar to those in the *dura mater* structure [8]. Arachnoid mater has been previously considered as part of the PM in mechanical testing while no clear evidence supported such assumption [12]. In our work, arachnoid was considered as part of the spinal *dura mater* as described in [11].

The PM structure has been described with fenestration in human cadaver's lumbar spine using histology and microscopy techniques. A large amount of collagen fibers as well as few elastin fibers were identified using staining. An amorphous intracellular substance, small vessels fibroblasts and macrophages were also identified. PM has several layers: subpial tissues with collagen fibers and pial cellular layers from neuroglial cells surrounding the spinal cord [8,13].

Such description of the meningeal tissues' structures highlights the difficulties associated with extraction. As previously underlined by Ramo et al. [4], there is a lack of description of the extraction process, in particular how to avoid tissue degeneration as well as a lack of knowledge on the conservation process [14].

1.2. Meningeal mechanical characterization

To define material properties, the experimental testing of the *dura mater* reported in the literature highly differs depending on the studied species and anatomical segments as well as on the objectives of the characterization protocol (description of quasi-static or dynamic behaviour of the tissue). Tensile test protocols have been mainly quasi-static or so and uni-axial. They were carried out on both brain and spinal *dura mater* samples from rats [15,16], canines [17], ovines [18], porcines [9,19], bovines [20–22] and humans [1,22–25]. More specific studies such as retraction of *dura mater* testing [16], *dura mater* relaxation [20] and fatigue ratio computation [9] as well as membrane inflation testing have also been reported [26]. Uni-axial quasi-static characterization of the meningeal tissue fails to predict the mechanical behaviour in a physiological context as physiological load in which both meningeal tissue directions are strained through the spinal cord motion and attachment itself as depicted in [27].

No clear consensus has been reached for the comparison of the *dura mater* mechanical behaviour with respect to the orientation of the tested tissue. Tensile strength and stiffness were found to be greater in the longitudinal direction than in the transverse/circumferential or coronal one [16,17,22,24]. However, the opposite results were also reported [20,21]. Such differences may be explained by the model used (human, canine or bovine) or the strain rate used in the protocols.

The literature reported differences in *dura mater* elastic modulus at different location along the spine in ovine [28] and porcine samples [19]. The latter study also showed a significant variability along the cervical segments and between ventral and dorsal sides of the spinal cord. A decrease of the tensile strength and of the elastic modulus with age has been reported

in rats [16] and cranial human *dura mater* [23]. Comparison among 0.01, 0.1 and 1 s^{-1} strain rates suggested no strain rate dependency [21], while a recent publication questioned such results [29].

Compared to the literature available on the properties of the *dura mater*, PM tissue has been far less characterized. Rabbit spinal PM was tested *in situ* using a tensile test of the spinal cord with computation of elastic modulus by comparison between intact and incised PM [30]. Atomic force microscopy was used with indentation and relaxation tests to characterize cortical and cerebellar PM in rats [31]. PM associated with brain white and grey matters has been studied in a bovine model with a strain rate of 10 s^{-1} and its quasi linear viscoelastic behaviour has been validated up to a strain level of 0.35% [32]. PM was also tested in bovine brains at three locations and with three different strain rates [12] using a shear test reproducing the relative motion between the inner skull and the brain, during a head impact, resulting in tangential shear loading on the PM layer [12]. Isolated bovine cranial PM was also tested in quasi-static tensile test (0.5 $mm.min^{-1}$) [33]. Using atomic force microscopy indentation in a rat PM and arachnoid complex (PAC), lower instantaneous Young modulus distribution was found in vascularized PAC when compared to non-vascularized tissue [31]. Finally, PAC was shown to have a strain rate dependent behaviour at strain rates of 0.05, 0.5, 5 and 100 s^{-1} in a bovine brain [34].

1.3. Bi-axial testing protocols

In the sub-arachnoidal canal, the spinal cord surrounded by PM is attached by its link to brain and along the spine by nerve roots and denticulate ligaments. Additionally, the mechanical support of arachnoid trabeculae has been studied in the human brain [35,36]. Sacks reported that bi-axial tensile tests providing the two dimensional stress-state enable constitutive modelling identification closer to physiological condition [37]. The spinal ovine *dura mater* and the human cranial vault *dura mater* have been for instance tested bi-axially, respectively by De Kegel et al. [38] and Shetye et al. [39].

Such tests allow the characterization of anisotropic biomaterials. However test systems and testing protocols differ from more classical uni-axial tests: gripping systems are usually different, as well as the pre-conditioning definition, the loading conditions and data analysis. Indeed, rake gripping systems were found to be less sensitive to the effects of boundary conditions when compared to clamp based methods [40]. Both available biaxial protocols were tested on *dura mater* [18,38] using different ratios of displacements between directions. The strain rate was 0.01 s^{-1} in [38] and not clearly mentioned in [18].

The influence of the method and duration of conservation (frozen, 24 h fresh; 120 h fresh and dry samples comparison) on mechanical properties was reported [22]. Conservation of the cranial *dura mater* was reported to be acceptable until a 139 h post mortem delay using a specific osmotic stress technique to adjust water content during conservation [23]. Other preservation conditions have been considered, such as storage in formalin [24], frozen conservation [41], glycerol conservation [25]. Considering such results and without the use of the osmotic stress technique, the time between death and the measurement of meningeal tissue mechanical characterisation should be limited to a maximum of 12 h.

1.4. Constitutive modelling

Constitutive modelling includes both phenomenological and structural modelling. It mostly consists in fitting Stress-Strain curves using constitutive strain energy models. Such constitutive models aim to describe typical mechanical behaviours such as non-linear elasticity, anisotropy and viscoelasticity of a material. The accuracy of the constitutive model used for the fitting process strongly depends on the choices and assumptions made in terms of boundary condition, types of fixation, and assumption about distortion or thickness approximation [42,43].

Several constitutive models have been developed to fit experimental behaviour of the *dura mater*. Among the simplest models, are the reduced relaxation function and the elastic response as in Haut et Little 1972 for collagen fiber [41], the Yeoh model that depends only on the first invariant of the Cauchy Green deformation tensor, or the Neo-Hookean model [38], the incompressible Ogden model (isotropic one-term hyper-elastic model with no viscous term depending on the strain rate) [15,21,38] or Mooney Rivlin and Skalak, Tozeren, Zarda and Chien (STZC) models [26] for incompressible hyper-elastic materials [9]. Among the most detailed and complex models, the incompressible Ogden model is an isotropic one-term hyper-elastic model that does not depend on the strain rate (no viscous term) [15,21,38]; the one proposed by Gasser et al. [18] is a transversely isotropic model but the authors propose also a formulation for anisotropic materials with two families of fibers: the Gasser-Ogden-Holzapfel (GOH) model and the reduced GOH model [38].

PM associated with arachnoid mater has been modelled as linear elastic [33,34], and more recently as nonlinear viscoelastic, transversely isotropic material via a Mooney-Rivlin material model for the ground matrix substance and a piecewise function for the strain energy function for fiber strengthening and fiber reinforcement [44]. An Ogden law was also used with two parameters as well as a three terms Generalized Rivlin formulation [32].

Finally, to summarize the previously described literature, bi-axial mechanical meningeal tissues testing has been limited, to the best of our knowledge, to two studies. The diversity of testing protocols (models, extraction methods, sample location, conservation techniques, testing system and strain rate) as well as post-processing methodologies (constitutive model to be used) makes it hard to compare obtained results. Thus, this work aims to provide a description and comparison of bi-axial mechanical testing of meningeal tissues. More especially, the aims of the present work are threefold:

1) To characterize the mechanical behaviour of the *dura mater* and arachnoid complex (DAC) and the *pia mater* (PM) of spinal porcine samples using quasi-static bi-axial tensile tests.
2) To investigate the micro-structures of the spinal DAC and PM samples using a two photon microscopy to provide the constitutive models with the number of fiber populations considered.
3) To identify the best suited constitutive models representing the behaviour of these materials by comparing previously offered constitutive models, and to determine the sets of parameters allowing to fit experimental data and quantify their variability.

2. Materials and methods

Based on histological investigations and previous work [14], the present study considers the arachnoid complex to be associated to the *dura mater* rather than the *pia mater* [4].

2.1. Dissection and extraction of the material

Eight complete spines were extracted from swine (40 to 50 kg, Landrace pigs, 3 to 4 months old). The samples were extracted post-mortem with respect for the European Convention on the protection of vertebrates used for experimental or other scientific purposes. Extraction took place at the C.E.R.C. (Centre d'Enseignement et de Recherche Chirurgical), Faculty of Medicine of Marseille, France, (government agreement number C-013-15-022 ; Ethical comitee CEEA 14). The method used for the sacrifice was the intravenous injection of pentobarbital and benzyl alcohol solution. The extraction took place less than half an hour after sacrifice. It was divided into three steps: the spine extraction itself, followed by the spinal cord removal from spinal canal, and sample preparation.

The meningeal tissues along the with spinal cord were carefully removed from the spinal canal using scalpels, gouge clamps, and small clamps. Then, the spine was cut through the intervertebral disks into four segments corresponding to cervical (C0-C7), upper thoracic (T1-

T7), lower thoracic (T8-T15) and lumbar segments (L1-L5; Figure 1-B). Sample preparation consisted of opening the *dura mater* on the lateral side, defined by the line between nerve roots. Identification of the tissue orientation was performed by sewing a thin 2-0 thread on the upper right nerve roots. PM removal was performed by sectioning the lateral side (the nerve roots line) and carefully pealing it out of the spinal cord using a sharp razor blade. The whole procedure was performed in a saline solution.

2.2. Bi-axial testing protocol

The bi-axial testing system used in this experiment was described in a previous work [45]. It consists of four synchronized and motorized arms, each equipped with one stepper motor (LSM025A-T4, step size of 0.047 µm, resolution 1/64 of a step, repeatability < 3 µm, accuracy of 15 µm , Zaber, Vancouver, Canada), allowing a maximum displacement of 25 mm each (Figure 2-A-B). The motors are driven by a dedicated card controlled by a QuantumX system (MX440, HBM, Darmstadt, Germany). Each arm is also equipped with a 50 N load cell (sensitivity of 0.001 N, total error of ±0.02%). The frequency of force reading is 140 Hz. Samples (size between 10 and 12 mm) are gripped with four rakes made of five "teeth" (Figure 2-C).

There is neither consensus nor clear recommendation on how pre-conditioning should be applied to the samples. In order to limited the test duration, pre-load was preferred to pre-conditioning. Pre-load was carried out by moving the motors at 0.05 $mm.s^{-1}$, and stopping them when the load reached 0.01 N.

Traction test to failure was then performed with the stepper motors controlled to have a displacement rate of 0.05 mm.s-1 with a ratio of (1:1) between the perpendicular direction. Such displacement rate was chosen as an intermediate between the physiological motion associated with the CSF and the physiological motion of the spine.

The initial distance between the two rakes facing each other was set at 7 mm and subsequently measured using an optical system.

The initial measurement of the sample was 7 by 7 mm. The initial thickness was measured using the method described in [14]. The samples were divided into 1mm by 10mm sections after fixation on an agar solution. Each section was pictured in micro-meter paper and the average of ten measurements of the section was calculated for each sample. A total of 30 measurements per tissue were averaged and its mean value was considered to be 0.21 mm for PM and 0.3 mm for DAC respectively, as suggested by (Sudres et al., 2020b). A stereo image acquisition system (two Phantom Miro C110 cameras, 12-bits 1.3 MPixel CMOS sensor, 915

fps at 1280 by 1024, Vision Research Phantom, Wayne, New Jersey, USA, 2 EFFI-SHARP-PWR-FL lights) coupled to a digital image correlation (DIC) software (VIC 3D, Correlated Solution, Irmo, SC 29063, USA) was used to capture local strain on the whole sample and study the failure of the specimens. Black paint (Rust oleum - oil-based paint spray) was sprayed onto the samples to get a speckle stochastic pattern without modifying the material properties of the tissue. The speckle dots created are themselves strained during deformation [48]. The image acquisition system was calibrated with a grid of 12 by 9 printed dots with a known distance of 2 mm between dots. The DIC post-processing included the computation of the local strain over a region of interest (subset size of 23 and step of 3). The experimental strain computation was first compared to the computation of the DIC local strain on a silicon membrane (see Section 8 - Supplementary Data 2). Samples were tested out of the water within 12h after sacrifice at room temperature and the time required to attach the sample to the testing system was minimized (less than 30 sec). The biological tissues were kept moisted by spraying water droplets onto the samples. Thirty-one DAC samples (8 cervical samples, 8 upper thoracic samples, 10 lower thoracic samples and 5 lumbar samples) and 26 PM samples (7 cervical samples, 9 upper thoracic samples, 5 lower thoracic samples and 5 lumbar samples) were tested during eight test sessions corresponding to each swine sacrifice.

2.3. Structural characterization

Microstructural investigation was conducted on 11 samples (6 DAC and 5 PM samples) extracted from one swine within 24 h after sacrifice. The samples investigated by microscopy were adjacent to the samples tested mechanically, extracted with the same method and of similar size. Indeed, due to the sample preparation to perform a microscopic investigation and the presence of paint as well as the deterioration of the tissue after the mechanical tests, the mechanically tested samples could not have been used for such an investigation. Sample preparation involved fixing the meningeal tissues (PM and DAC samples) in agarose solution without covering the tissue in Petri boxes. Orientation of the samples in the agarose was such that the longitudinal axis corresponded to the y-axis and the circumferential axis to the x-axis. The samples were kept at all time in a controlled environment (immerged in saline solution at 4 °C). The multi-photon microscopy system was a Zeiss LSM 780 2P with five NDD gASP detectors with two-photon imaging system to detect type II collagen. This system produced stacks of images with an in plane resolution of 0.42 by 0.42 µm and a slice thickness between 5 µm and 10 µm. The laser wavelength was set to 860 nm with a power of 25 to 70%

depending on the tissue. The power tended to be higher for *pia mater*: pixel time was 6.3 µs, line time 0.35 µs and frame time 30.98 s.

The density and orientation of collagen fibers depend on the structure (PM and DAC). However, PM and DAC have a different arrangement of collagen fibers, varying with the location of the tissue (anterior or posterior) and the spinal location. Three locations were selected within the sample and for each location, three specific fibers were selected to be representative of the different orientations found in the tissue (as different as possible). The structural and geometrical characterization of the fiber was investigated using Dragonfly software (Object Research Systems (ORS) Inc., Montréal, CA). Collagen fibers have a sinusoidal wavy shape. Thus, a geometrical description of the selected fiber consists in three width (half period, ½ P) values and three peak amplitudes of the sinusoidal shape, the fibers thickness, and the fiber length and orientation defined as an orientation reference (straight line through the sinusoidal signal, orientation as an angle with the x-direction vector). Fiber volume fraction is computed as a substitute for fiber density (the percentage of a segmentation of fibers using automatic Otsu method over the whole volume of the scanned sample). A semi-quantitative method was used (i.e. it aimed to depict the variability of the fibers found in the tissue to explain anisotropy rather than to quantitatively and statistically compare and define the whole structure).

2.4. Data analysis and statistical analysis

The engineering stress was computed as the ratio of the tensile force and the initial cross-section area computed as the rake-to-rake width multiplied by averaged tissue thickness. Engineering strain on each axis was computed as the elongation at time *t* along one axis direction divided by the initial length in this direction (data from displacement sensor, comparison between sensor and DIC measurement on artificial material). Bi-linear fitting of the four Stress-Strain curves was performed using Matlab, including signal processing and optimization toolbox (2019b, The Matworks, Natik, Massachusetts, US) after registration of the curves. Failure detection was performed using peak detection of the second derivative of the computed StressStraincurve. Toe strain, toe stress, and elastic modulus were computed using a polyfit Matlab function (Figure 3). Toe stress and strain were computed maximizing r^2 of both toe and elastic region fits and elastic modulus resulted in the slope of the resulting fit corresponding to the elastic region.

The different constitutive models implemented in Matlab for the post-processing of the experimental data are summarized in Table 1 and details on constitutive models can be found

in section 8 (supplementary data). Parameter fitting was performed on each pair of experimental curves (circumferential and longitudinal curves taken during the same experiment) and the resulting parameters were averaged with computed standard deviation.

Statistical analysis was performed using the R language (CRAN, R project, [49]). Normality of the distribution was tested using a Shapiro-Wilk test. As p value of the Shapiro-Wilk test was found to be inferior to 0.05, hypothesis of normality of the result distributions was rejected. Thus, a Wilcoxon test was used to test differences between the two orientations of the samples (paired) as well as between spinal locations (not paired). Kruskal-Wallis (not paired) was used to test the influence of the spinal location on the different material characteristics. Significance level was defined at 5%. r^2 (eqn 13) and RMSE (eqn 14) of the fit between experimental data and model data were computed respectively as:

$$r^2 = 1 - \sum_{\text{i in mes}} \frac{f(x) - y_i}{\sqrt{(\hat{y} - y_i)^2}} \qquad \text{(eqn 13)}$$

$$RMSE = \sqrt{\sum_{\text{i in mes}} \frac{(\hat{y} - y_i)^2}{n}} \qquad \text{(eqn 14)}$$

With $\hat{y}$ the mean of the initial value, y_i the experimental value and f(x) the fitted function; i in measurements (Figure 3).

As previously described in [14], Bayesian linear mixed models were used to take into account the between-subjects and within-subjects variabilities in the elastic modulus results in reporting standard error (SE) associated with local elastic moduli.

3. Results

3.1. DAC mechanical characterization

Longitudinal elastic moduli were found to be significantly higher than circumferential ones at all locations ($p<0.001$, Table 3). Toe and failure stresses were also found to be significantly different ($p<0.005$ and $p<0.001$ respectively) with a higher value of both strain and stress at failure for longitudinal DAC (Figure 4). The Stress-Strain curves do not show any trend with respect to the spinal location.

Constitutive modelling fitting showed similar results for the anisotropic GOH model, Transverse isotropic Gasser model, and anisotropic Gasser model ($r^2=0.99$ for all, and respectively, RMSE of 0.4±0.3, 0.4±0.3 and 0.3±0.2 MPa – Table 2). The best fits were obtained with the anisotropic Gasser model. When using this model and comparing the two

described fibers populations, the fibers population parameters were found significantly different between κ_1 and κ_2, and between β and γ ($p<0.001$).

3.2. PM mechanical characterization

Elastic moduli, toe and failure stresses were found significantly different between circumferential and longitudinal directions for the PM ($p<0.001$, $p<0.02$ and $p<0.001$, respectively - Table 3). Stress-Strain curves of longitudinal PM samples appear to be grouped by spinal location (Figure 4). Supplementary Figure 1 depicts the average curves by spinal location, but they are strongly influenced by results from each of the single curve so parameter fitting using the pair of circumferential and longitudinal curves should be preferred as in Table 3. The anisotropic GOH and the transverse isotropic and anisotropic Gasser models presented the best fit compared to the other constitutive models. For the anisotropic Gasser model, fibers population parameters were found significantly different in average for all parameters (k_1 and k_3: $p\leq0.005$, k_2 and k_4: $p\leq0.03$, κ_1 and κ_2, and β and γ: $p<0.001$).

3.3. Differences in spinal location

The study of the influence of sample location in the spine is depicted in Table 4. The Kruskal-Wallis test did not reveal any significant influence of the spinal location. When comparing location by location, the longitudinal elastic moduli were found higher on average in the upper thoracic spine and cervical spine than in the lower locations, while the cervical and upper thoracic circumferential elastic moduli were similar. In both directions, DAC elastic moduli decrease towards the lower spine. Similar results are found for PM in the longitudinal direction, while lumbar circumferential elastic moduli were higher than in the low thorax. Differences between directions in elastic moduli were significant for DAC at all locations except for the cervical spine ($p\leq0.08$) while differences in PM were only significant for the cervical and thoracic locations.

Comparing the spine locations, significant differences were found for the circumferential elastic moduli of the PM between upper and lower thorax, for the longitudinal failure stresses between high and low thorax for the DAC and for failure stresses between cervical and low thorax and cervical and lumbar spine in both directions for the PM. Similar trends were observed for the longitudinal DAC sample, although not significant ($p\leq0.054$).

3.4. Fiber structure

In DAC, the tissue mainly showed highly curled collagen fibers (Figure 5), which are present in high density within the sample. Two photon images showed that the collagen fibers in the DAC changed within the same sample (anterior and posterior), with different orientations and

structures. In the PM, fiber orientation is depicted in Figure 6. Fenestrations can be observed in the PM structure as well as vascularization (Figure 6-E and F).

A semi quantitative description of the fiber structures can be found in Table 5. At all spine locations, DAC image show variability in the fiber orientation within the same sample. It presented a volume fraction, fiber thickness and width increase depicting changes in micro-structure organisation between spinal locations. PM fibers orientation is found to vary both within the same sample and along the spine. The half -amplitude of the collagen fiber curl is higher in the PM than in the DAC. The fiber volume fraction used to depict the density of fibers slightly varies between 17.3% and 25.4% (thoracic).

4. Discussion

This study investigated the material properties of the meningeal tissue in a swine model with the perspective of testing the constitutive models previously described in the literature. The ultimate goal was to fully describe the behaviour of such material. Two fibers population models presented better results for DAC. The anisotropic Gasser model parameters found significant differences between fiber population descriptions (fibers dispersion coefficient and orientation). Indeed, micro-structural investigation showed a high variability of fibers orientation within a same sample without a clear identification of two fiber populations. This study is the first, to the authors' knowledge, to report biaxial tensile test of the PM and to provide constitutive modelling for such tests. The anisotropic Gasser model presented a slightly better fit for PM with significant differences in parameters descriptions of all fiber populations.

4.1. DAC characterization and constitutive parameters fitting

In this biaxial tensile test study of porcine DAC, the elastic modulus of longitudinal DAC (108.1±40.3 MPa) was found higher than circumferential (53.2±31.7 MPa, $p<0.001$). This has been previously reported and has been explained by the fiber organisation [10,47]. Such an explanation is supported by our micro-structural investigation using the two photon microscopy (fiber orientation between 2.55 to 4.77 radiant from the circumferential direction). However, the orientation of the fiber population identified in the constitutive models was found between 0.76±0.67 and 0.87±0.74 radiant. The dispersion of our results, illustrated by a large standard deviation, can be explained by the fact that samples were taken at different locations of the spine.

Wide ranges of values have been found in the literature in terms of elastic moduli for uni-axial tensile tests. Such values are 7.5 - 26 MPa [9]; 3.3 - 7.9 MPa [50]; 44 - 91 MPa in fossa

human sample dural (strain rate of 1.5 X 10^{-3} s^{-1}) [1]; 70 ± 44 MPa [23] 25 - 70 MPa [22] in the cranial bovine longitudinal *dura mater*. In the human spine and in the different orientation: elastic moduli in the longitudinal direction was reported to be 62 - 102 MPa [22] and 138 - 265 MPa [17] vs in the circumferential direction, 4 - 8 MPa [22] and 7.8 - 76.4 MPa [17]. When comparing uni-axial results with biaxial, the difference in ratio between circumferential and longitudinal elastic moduli should be noticed. It appears that applying a second loading in the perpendicular direction accentuates the differences in material behaviour in the two directions as suggested in [51].Thus, no consensus on the comparison of stiffness between circumferential and longitudinal directions for DAC tissue was reached [18,20,21,52] depending of the location of DAC sample extraction (between cranial or spinal locations).

In biaxial testing, the DAC elastic modulus was found to be higher in the circumferential direction compared to in the longitudinal one [18] in an ovine spinal cord. Also, a difference in compliance was found between the two directions in the toe region only [53] while thickness is reported to compensate for the change in material properties. Similar trends were found in our work (significant different $p \leq 0.02$ between longitudinal and circumferential toe stress and higher toe stress for thoracic compared to lumbar samples). These differences within the literature could be explained by the fact that the strain rates are not mentioned in most of articles. The testing conditions may therefore be slightly different. It is to be noted, that when comparing parameters in the different Gasser constitutive models, similar orientations were found (0.17±0.26 radiant and 1.42±1.06 radiant for anisotropic Gasser model and 1.51±0.32 radiant for Trans. Iso. Gasser model in a cervical ovine spine [18].

Our comparison between constitutive models reported slightly higher results for the anisotropic Gasser model with two fiber population models when focusing on RMSE (0.27 MPa vs 0.44 MPa). RMSE values were higher than the ones found by Shetye et al. [18]. Our results are in line with the recommendation to use anisotropic two fiber family continuum model from this previous study. Additionally, significant differences in orientation and dispersion coefficient between the two fiber populations were also found while not confirming significant differences between non-linearity coefficients (k_2 and k_4). Such difference could result from differences in maximum loading, strain rate testing conditions as well as post-processing methodology (fitting on each experimental curve vs fitting on the average curve) and sample locations and animal model (ovine cervical only samples in Shetye et al. [18]). When detailing result by spinal location and differentiating high and low thorax (Supplementary data 3), all parameters differ according with spinal location which could

explain the large variation found in the result. As specified in limitation, such results need further investigation.

According with inverse analysis reported by Laville et al. [45], further studies including several ratio of testing conditions could lead to the evolution of identified parameters. Indeed, when more ratios are tested, one axis will reach the set force threshold and stop before the other which could lead to fiber rotation [45]. Additionally, a full simulation of the experiment by a finite element model and an optimization process to fit parameters could further investigate the biaxial behaviour of the tissue while avoiding the risk associated with local minims.

4.2. PM and constitutive parameters fitting

Elastic moduli determined by biaxial tensile tests in PM samples were found significantly different between longitudinal and circumferential directions (26.3±13.3 MPa and 12.9±8.7 MPa, respectively). This study is the first to present biaxial testing of the PM tissue. The presented values are higher than those reported in the literature for uni-axial traction testing. Tensile elastic modulus of bovine cranial PM was found to be 19 kPa [33] and 2300 kPa in spinal rabbit PM (spinal cord tensile test with and without PM) [54]. Also, vascularized and non-vascularized tissue elastic modulus were compared (2.79±0.08 kPa and 1.32±0.03 kPa) [31]. Such differences could be explained by the animal model differences as well as the location of the extracted samples.

No advantages were found for the Mooney-Rivlin based material model with fiber strengthening when compared to transversely anisotropic material or fiber population models. When focusing on the anisotropic Gasser model, non-linearity of the two fibers populations were found significantly different for all parameters of the fiber population description. Micro-structural investigation showed that fenestration could also be taken into consideration when modelling the PM through fiber volume fraction.

While PM (or more precisely PAC according to the authors' hypothesis) was previously described by Jin et al. [44] with a Mooney Rivlin model that included a piecewise function to consider the fibers strengthening, our results suggest the use of an Anisotropic Gasser model which fully described two different fibers populations. The results on collagen fiber structures suggest that a further investigate be performed where fenestration should be considered in the constitutive modelling.

4.3. Testing protocols and limitations

Despite the relevant results presented, this study has some limitations.

Additional testing conditions could have been tested in all samples, however the conservation time after sacrifice was critical, and determining viscoelasticity properties of the meningeal tissues was out of the scope of this work. Further studies are required for the investigations of *pia* and *pia mater* viscoelasticity such as described in other biological materials [55]. Further investigations should also include different displacement rates as strongly advised in other studies [56], [45]. In the later study [45], an inverse analysis approach using finite element modelling showed that at least three experimental loading conditions are necessary to find a set of parameters that allows other loading conditions to be modelled. This is to limit the risks of non-uniqueness of solutions. In the present study, this problem was solved by fitting the parameters on all available experimental data rather than fitting parameters on an average curve. Such a design of experiment was also chosen to conduct rupture testing to be able to define a force threshold to be reached without sample damage.

Additionally, as reported in [52], the bulge inflation testing could also have been used to test multiaxially the meningeal tissue and closely mimicking *in-vivo* conditions while relating pressure to stress and deflection to strain.

Other issues are as follows. Depending on the biological tissues tested, pre-conditioning methods can be expressed as a percentage of initial length, as a percentage of the maximal strain or stretch or as a maximum strain value [46]. It has been shown that pre-conditioning less than 1% circumferential and 3% longitudinal of the maximum force does not alter the mechanical behaviour of the tissue but allows for better positioning of the sample on its support and stabilizes the test [20]. Pre-conditioning could have been added. Additional testing conditions could have been performed in terms of direction ratio and strain rate. The use of black paint to create a stochastic speckle pattern could be changed to coloration of existing surface features in order to avoid addition of material preventing further microscopic analysis. Quantification of the collagen fibers and could have been considered directly on the tested sample, as described in a different application [57]; however, access to the imaging facilities associated with the same day of sacrifice was not possible. A full characterization of the collagen on tested samples could also be considered as well as further investigation of other components of the tissue such as elastin fibers. In addition, usefulness of a swine model could be questioned as quadruped morphology probably implied different organization of the tissue, availability of testing material is a non-negligible advantage and the lack of data of such meningeal tissue mechanical characterization made it acceptable. Constitutive models could then be investigated using finite element modelling [42] with inverse analysis, and this could facilitate further transition to spinal cord compression modelling [58,59].

5. Conclusion

This study presented significant differences in elastic moduli of circumferential and longitudinal directions in both DAC and PM tissues when tested using bi-axial tensile tests. Significant differences were found between circumferential PM low and high thorax while changes of material properties along the spinal cord were not found significant. Comparison between constitutive models showed that the anisotropic Gasser constitutive model seems to be the best suited one for both DAC and PM. The micro-structural description enabling discussion on the capacity of constitutive law theory to match micro-structure description of meningeal tissues.

6. Acknowledgements

The authors would like to thank Anthony Melot for his great help on swine dissection, Frédéric Brocard for the two photon imaging and Christophe Pradille for the development of, and his assistance in, the use bi-axial test system. This study was supported by the Champlain/ AIMCI fellowship.

7. Declaration of Competing Interest

The authors declare to have no conflict of interest associated with this study.

8. References

[1] D. Chauvet, A. Carpentier, J.-M. Allain, M. Polivka, J. Crépin, B. George, Histological and biomechanical study of dura mater applied to the technique of dura splitting decompression in Chiari type I malformation., Neuro Surg. Rev. 33 (2010) 287–94; discussion 295. https://doi.org/10.1007/s10143-010-0261-x.

[2] M. Protasoni, S. Sangiorgi, A. Cividini, G.T. Culuvaris, G. Tomei, C. Dell'Orbo, M. Raspanti, S. Balbi, M. Reguzzoni, The collagenic architecture of human dura mater, J. Neurosurg. 114 (2011) 1723–1730. https://doi.org/10.3171/2010.12.JNS101732.

[3] K.D. Fong, S.M. Warren, E.G. Loboa, J.H. Henderson, T.D. Fang, C.M. Cowan, D.R. Carter, M.T. Longaker, Mechanical strain affects dura mater biological processes: implications for immature calvarial healing, Plast. Reconstr. Surg. 112 (2003) 1312–1327. https://doi.org/10.1097/01.PRS.0000079860.14734.D6.

[4] N.L. Ramo, K.L. Troyer, C.M. Puttlitz, Viscoelasticity of spinal cord and meningeal tissues., Acta Biomater. 75 (2018) 253–262. https://doi.org/10.1016/j.actbio.2018.05.045.

[5] C.D. Bertram, Evaluation by fluid/structure-interaction spinal-cord simulation of the effects of subarachnoid-space stenosis on an adjacent syrinx, J. Biomech. Eng. 132 (2010) 061009. https://doi.org/10.1115/1.4001165.

[6] C.D. Bertram, M. Heil, A Poroelastic Fluid/Structure-Interaction Model of Cerebrospinal Fluid Dynamics in the Cord With Syringomyelia and Adjacent Subarachnoid-Space Stenosis, J. Biomech. Eng. 139 (2017). https://doi.org/10.1115/1.4034657.

[7] M.S. Sacks, W. Sun, Multiaxial mechanical behavior of biological materials, Annu. Rev. Biomed. Eng. 5 (2003) 251–284. https://doi.org/10.1146/annurev.bioeng.5.011303.120714.

[8] M.A. Reina, O.D.L. De León Casasola, M.C. Villanueva, A. López, F. Machés, J.A. De Andrés, Ultrastructural findings in human spinal pia mater in relation to subarachnoid anesthesia, Anesth. Analg. 98 (2004) 1479–1485, table of contents. https://doi.org/10.1213/01.ane.0000113240.09354.e9.

[9] D.R. Walsh, A.M. Ross, S. Malijauskaite, B.D. Flanagan, D.T. Newport, K.D. McGourty, J.J.E. Mulvihill, Regional mechanical and biochemical properties of the porcine cortical meninges, Acta Biomater. 80 (2018) 237–246. https://doi.org/10.1016/j.actbio.2018.09.004.

[10] A. Kinaci, W. Bergmann, R. Bleys, A. van der Zwan, T. van Doormaal, Histologic Comparison of the Dura Mater among Species., Comp. Med. 70 (2020) 170–175. https://doi.org/10.30802/aalas-cm-19-000022.

[11] M.A. Reina, A. Boezaart, C. De Andres-Serrano, R. Rubio-Haro, J. De Andrés, Microanatomy Relevant to Intrathecal Drug Delivery, Methods Mol. Biol. Clifton NJ. 2059 (2020) 109–120. https://doi.org/10.1007/978-1-4939-9798-5_4.

[12] X. Jin, K.H. Yang, A.I. King, Mechanical properties of bovine pia-arachnoid complex in shear, J. Biomech. 44 (2011) 467–474. https://doi.org/10.1016/j.jbiomech.2010.09.035.

[13] F. Machés, M.A. Reina, O. De León Casasola, Ultrastructure of Spinal Pia Mater, in: M.A. Reina, J.A. De Andrés, A. Hadzic, A. Prats-Galino, X. Sala-Blanch, A.A.J. van Zundert (Eds.), Atlas Funct. Anat. Reg. Anesth. Pain Med. Hum. Struct. Ultrastruct. 3D Reconstr. Images, Springer International Publishing, Cham, 2015: pp. 499–522. https://doi.org/10.1007/978-3-319-09522-6_25.

[14] P. Sudres, M. Evin, E. Wagnac, N. Bailly, L. Diotalevi, A. Melot, P.-J. Arnoux, Y. Petit, Tensile mechanical properties of the cervical, thoracic and lumbar porcine spinal meninges, J. Mech. Behav. Biomed. Mater. 115 (2021) 104280. https://doi.org/10.1016/j.jmbbm.2020.104280.

[15] J.T. Maikos, R.A.I. Elias, D.I. Shreiber, Mechanical properties of dura mater from the rat brain and spinal cord, J. Neurotrauma. 25 (2008) 38–51. https://doi.org/10.1089/neu.2007.0348.

[16] J.H. Henderson, R.P. Nacamuli, B. Zhao, M.T. Longaker, D.R. Carter, Age-dependent residual tensile strains are present in the dura mater of rats, J. R. Soc. Interface. 2 (2005) 159–167. https://doi.org/10.1098/rsif.2005.0035.

[17] D.J. Patin, E.C. Eckstein, K. Harum, V.S. Pallares, Anatomic and biomechanical properties of human lumbar dura mater, Anesth. Analg. 76 (1993) 535–540. https://doi.org/10.1213/00000539-199303000-00014.

[18] S.S. Shetye, M.M. Deault, C.M. Puttlitz, Biaxial response of ovine spinal cord dura mater, J. Mech. Behav. Biomed. Mater. 34 (2014) 146–153. https://doi.org/10.1016/j.jmbbm.2014.02.014.

[19] E. Mazgajczyk, K. Ścigała, M. Czyż, W. Jarmundowicz, R. Będziński, Mechanical properties of cervical dura mater, Acta Bioeng. Biomech. 14 (2012) 51–58.

[20] R.K. Wilcox, L.E. Bilston, D.C. Barton, R.M. Hall, Mathematical model for the viscoelastic properties of dura mater, J. Orthop. Sci. Off. J. Jpn. Orthop. Assoc. 8 (2003) 432–434. https://doi.org/10.1007/s10776-003-0644-9.

[21] C. Persson, S. Evans, R. Marsh, J.L. Summers, R.M. Hall, Poisson's ratio and strain rate dependency of the constitutive behavior of spinal dura mater, Ann. Biomed. Eng. 38 (2010) 975–983. https://doi.org/10.1007/s10439-010-9924-6.

[22] M. Runza, R. Pietrabissa, S. Mantero, A. Albani, V. Quaglini, R. Contro, Lumbar dura mater biomechanics: experimental characterization and scanning electron microscopy observations, Anesth. Analg. 88 (1999) 1317–1321. https://doi.org/10.1097/00000539-199906000-00022.

[23] J. Zwirner, M. Scholze, J.N. Waddell, B. Ondruschka, N. Hammer, Mechanical Properties of Human Dura Mater in Tension – An Analysis at an Age Range of 2 to 94 Years, Sci. Rep. 9 (2019) 1–11. https://doi.org/10.1038/s41598-019-52836-9.

[24] E. Zarzur, Mechanical properties of the human lumbar dura mater, Arq. Neuropsiquiatr. 54 (1996) 455–460. https://doi.org/10.1590/s0004-282x1996000300015.

[25] R. van Noort, M.M. Black, T.R. Martin, S. Meanley, A study of the uniaxial mechanical properties of human dura mater preserved in glycerol, Biomaterials. 2 (1981) 41–45. https://doi.org/10.1016/0142-9612(81)90086-7.

[26] T.J. Kriewall, N. Akkas, D.I. Bylski, J.W. Melvin, B.A. Work, Mechanical behavior of fetal dura mater under large axisymmetric inflation, J. Biomech. Eng. 105 (1983) 71–76. https://doi.org/10.1115/1.3138388.

[27] P. Sudres, M. Evin, P.-J. Arnoux, V. Callot, Cervical canal morphology: Effects of neck flexion in normal condition - New elements for biomechanical simulations and surgical management, Spine. (2020). https://doi.org/10.1097/BRS.0000000000003496.

[28] C. Yang, X. Yang, X. Lan, H. Zhang, M. Wang, Y. Zhang, Y. Xu, P. Zhen, [Structure and mechanical characteristics of spinal dura mater in different segments of sheep's spine], Zhongguo Xiu Fu Chong Jian Wai Ke Za Zhi Zhongguo Xiufu Chongjian Waike Zazhi Chin. J. Reparative Reconstr. Surg. 33 (2019) 232–238. https://doi.org/10.7507/1002-1892.201807085.

[29] N. Ramo, S.S. Shetye, C.M. Puttlitz, Damage Accumulation Modeling and Rate Dependency of Spinal Dura Mater, J. Eng. Sci. Med. Diagn. Ther. 1 (2017). https://doi.org/10.1115/1.4038261.

[30] H. Ozawa, T. Matsumoto, T. Ohashi, M. Sato, S. Kokubun, Mechanical properties and function of the spinal pia mater, J. Neurosurg. Spine. 1 (2004) 122–127. https://doi.org/10.3171/spi.2004.1.1.0122.

[31] G. Fabris, Z. M. Suar, M. Kurt, Micromechanical heterogeneity of the rat pia-arachnoid complex, Acta Biomater. 100 (2019) 29–37. https://doi.org/10.1016/j.actbio.2019.09.044.

[32] K. Laksari, M. Shafieian, K. Darvish, Constitutive model for brain tissue under finite compression, J. Biomech. 45 (2012) 642–646. https://doi.org/10.1016/j.jbiomech.2011.12.023.

[33] P. Aimedieu, R. Grebe, Tensile strength of cranial pia mater: preliminary results, J. Neurosurg. 100 (2004) 111–114. https://doi.org/10.3171/jns.2004.100.1.0111.

[34] X. Jin, J.B. Lee, L.Y. Leung, L. Zhang, K.H. Yang, A.I. King, Biomechanical response of the bovine pia-arachnoid complex to tensile loading at varying strain-rates, Stapp Car Crash J. 50 (2006) 637–649.

[35] N. Benko, E. Luke, Y. Alsanea, B. Coats, Spatial distribution of human arachnoid trabeculae, J. Anat. 237 (2020) 275–284. https://doi.org/10.1111/joa.13186.

[36] M.M. Mortazavi, S.A. Quadri, M.A. Khan, A. Gustin, S.S. Suriya, T. Hassanzadeh, K.M. Fahimdanesh, F.H. Adl, S.A. Fard, M.A. Taqi, I. Armstrong, B.A. Martin, R.S. Tubbs, Subarachnoid Trabeculae: A Comprehensive Review of Their Embryology, Histology, Morphology, and Surgical Significance, World Neurosurg. 111 (2018) 279–290. https://doi.org/10.1016/j.wneu.2017.12.041.

[37] M.S. Sacks, Biaxial Mechanical Evaluation of Planar Biological Materials, J. Elast. Phys. Sci. Solids. 61 (2000) 199. https://doi.org/10.1023/A:1010917028671.

[38] D. De Kegel, J. Vastmans, H. Fehervary, B. Depreitere, J. Vander Sloten, N. Famaey, Biomechanical characterization of human dura mater, J. Mech. Behav. Biomed. Mater. 79 (2018) 122–134. https://doi.org/10.1016/j.jmbbm.2017.12.023.

[39] S.S. Shetye, M.M. Deault, C.M. Puttlitz, Biaxial response of ovine spinal cord dura mater, J. Mech. Behav. Biomed. Mater. 34 (2014) 146–153. https://doi.org/10.1016/j.jmbbm.2014.02.014.

[40] W. Sun, M.S. Sacks, M.J. Scott, Effects of boundary conditions on the estimation of the planar biaxial mechanical properties of soft tissues, J. Biomech. Eng. 127 (2005) 709–715. https://doi.org/10.1115/1.1933931.

[41] R.C. Haut, R.W. Little, A constitutive equation for collagen fibers, J. Biomech. 5 (1972) 423–430. https://doi.org/10.1016/0021-9290(72)90001-2.

[42] H. Fehervary, M. Smoljkić, J. Vander Sloten, N. Famaey, Planar biaxial testing of soft biological tissue using rakes: A critical analysis of protocol and fitting process, J. Mech. Behav. Biomed. Mater. 61 (2016) 135–151. https://doi.org/10.1016/j.jmbbm.2016.01.011.

[43] N.T. Jacobs, D.H. Cortes, E.J. Vresilovic, D.M. Elliott, Biaxial tension of fibrous tissue: using finite element methods to address experimental challenges arising from boundary conditions and anisotropy, J. Biomech. Eng. 135 (2013) 021004. https://doi.org/10.1115/1.4023503.

[44] X. Jin, H. Mao, K.H. Yang, A.I. King, Constitutive modeling of pia-arachnoid complex, Ann. Biomed. Eng. 42 (2014) 812–821. https://doi.org/10.1007/s10439-013-0948-6.

[45] C. Laville, C. Pradille, Y. Tillier, Mechanical characterization and identification of material parameters of porcine aortic valve leaflets, J. Mech. Behav. Biomed. Mater. (2020) 104036. https://doi.org/10.1016/j.jmbbm.2020.104036.

[46] V. Deplano, M. Boufi, O. Boiron, C. Guivier-Curien, Y. Alimi, E. Bertrand, Biaxial tensile tests of the porcine ascending aorta, J. Biomech. 49 (2016) 2031–2037. https://doi.org/10.1016/j.jbiomech.2016.05.005.

[47] P. Sudres, M. Evin, E. Wagnac, N. Bailly, L. Diotalevi, E. Laroche, A. Melot, P.-J. Arnoux, Y. Petit, Quasi-Static Tensile Mechanical Properties of the Porcine Spinal Meninges, Submitt. J. Mech. Behav. Biomed. Mater. (2020).

[48] M. Palanca, G. Tozzi, L. Cristofolini, The use of digital image correlation in the biomechanical area: a review, Int. Biomech. 3 (2016) 1–21. https://doi.org/10.1080/23335432.2015.1117395.

[49] R Core Team, R: A Language and Environment for Statistical Computing, R Foundation for Statistical Computing, Vienna, Austria, 2020. https://www.R-project.org/.

[50] R. van Noort, M.M. Black, T.R. Martin, S. Meanley, A study of the uniaxial mechanical properties of human dura mater preserved in glycerol, Biomaterials. 2 (1981) 41–45. https://doi.org/10.1016/0142-9612(81)90086-7.

[51] A. Mauri, S.M. Zeisberger, S.P. Hoerstrup, E. Mazza, Analysis of the uniaxial and multiaxial mechanical response of a tissue-engineered vascular graft, Tissue Eng. Part A. 19 (2013) 583–592. https://doi.org/10.1089/ten.tea.2012.0075.

[52] B. Pierrat, L. Carroll, F. Merle, D.B. MacManus, R. Gaul, C. Lally, M.D. Gilchrist, A. Ní Annaidh, Mechanical Characterization and Modeling of the Porcine Cerebral Meninges, Front. Bioeng. Biotechnol. 8 (2020) 801. https://doi.org/10.3389/fbioe.2020.00801.

[53] A. Tamura, W. Yano, D. Yoshimura, S. Nishikawa, Mechanical characterization of spinal dura using a pd-controlled biaxial tensile tester, J. Mech. Med. Biol. 20 (2020) 2050023. https://doi.org/10.1142/S0219519420500232.

[54] H. Ozawa, T. Matsumoto, T. Ohashi, M. Sato, S. Kokubun, Mechanical properties and function of the spinal pia mater, J. Neurosurg. Spine. 1 (2004) 122–127. https://doi.org/10.3171/spi.2004.1.1.0122.

[55] A. Anssari-Benam, Y.-T. Tseng, G.A. Holzapfel, A. Bucchi, Rate-dependency of the mechanical behaviour of semilunar heart valves under biaxial deformation, Acta Biomater. 88 (2019) 120–130. https://doi.org/10.1016/j.actbio.2019.02.008.

[56] S. Budday, G. Sommer, C. Birkl, C. Langkammer, J. Haybaeck, J. Kohnert, M. Bauer, F. Paulsen, P. Steinmann, E. Kuhl, G.A. Holzapfel, Mechanical characterization of human brain tissue, Acta Biomater. 48 (2017) 319–340. https://doi.org/10.1016/j.actbio.2016.10.036.

[57] J. Brunet, B. Pierrat, P. Badel, Review of current advances in the mechanical description and quantification of aortic dissection mechanisms, IEEE Rev. Biomed. Eng. (2020). https://doi.org/10.1109/RBME.2019.2950140.

[58] S. Jannesar, B. Nadler, C.J. Sparrey, The Transverse Isotropy of Spinal Cord White Matter Under Dynamic Load, J. Biomech. Eng. 138 (2016) 091004–091004. https://doi.org/10.1115/1.4034171.

[59] H. Kimpara, Y. Nakahira, M. Iwamoto, K. Miki, K. Ichihara, S. Kawano, T. Taguchi, Investigation of anteroposterior head-neck responses during severe frontal impacts using a brain-spinal cord complex FE model, Stapp Car Crash J. 50 (2006) 509–544.

2. Figures and Tables

Figure 1 – Components of the extracted segments (A) with spine segment location (B), spinal cord extraction (C and D)

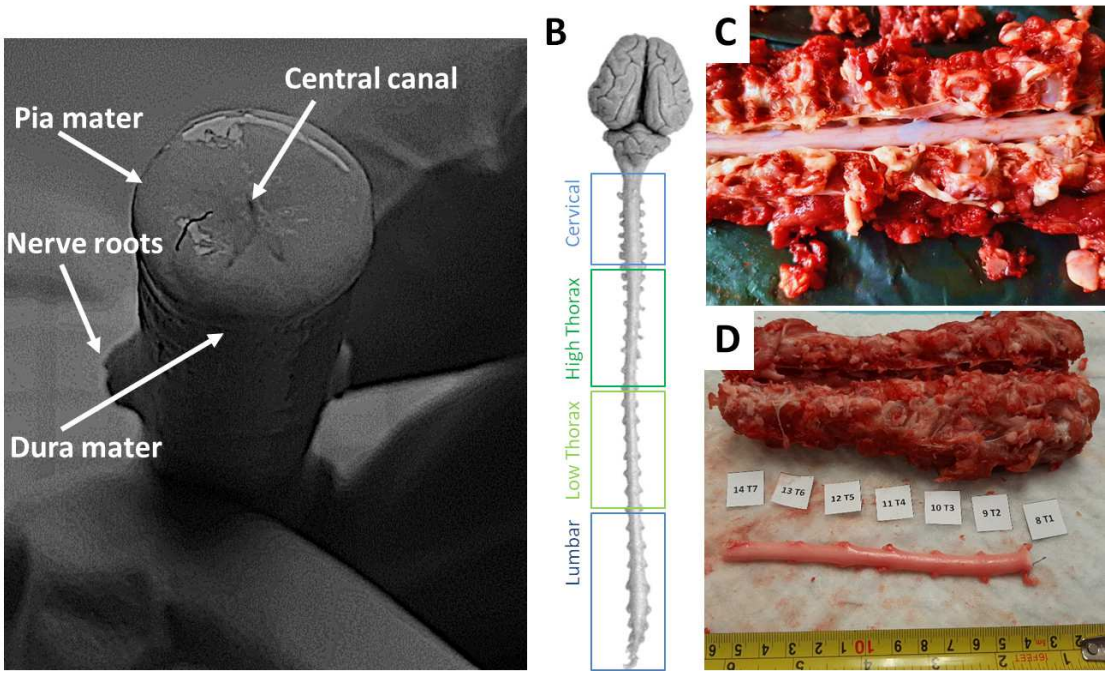

Figure 2 – Biaxial sample (A), custom made test system (B) and details of the system (C).

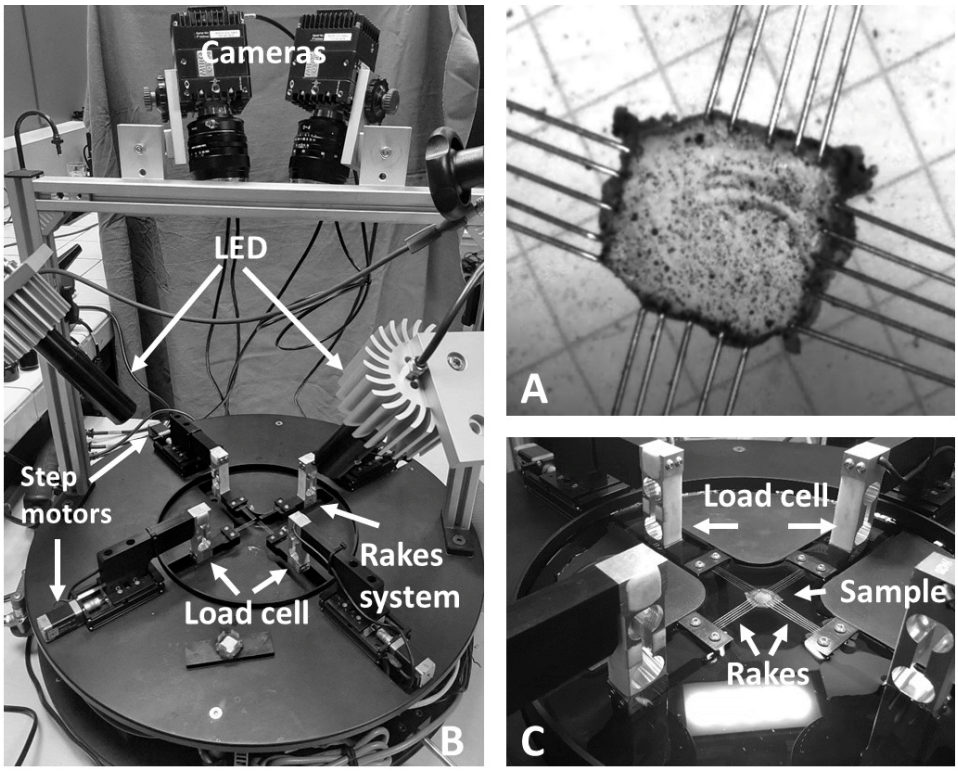

Figure 3 – Example of bi-linear curve fitting for identification of toe region and elastic modulus computation (A) and anisotropic Gasser model fit for a DAC sample (B).

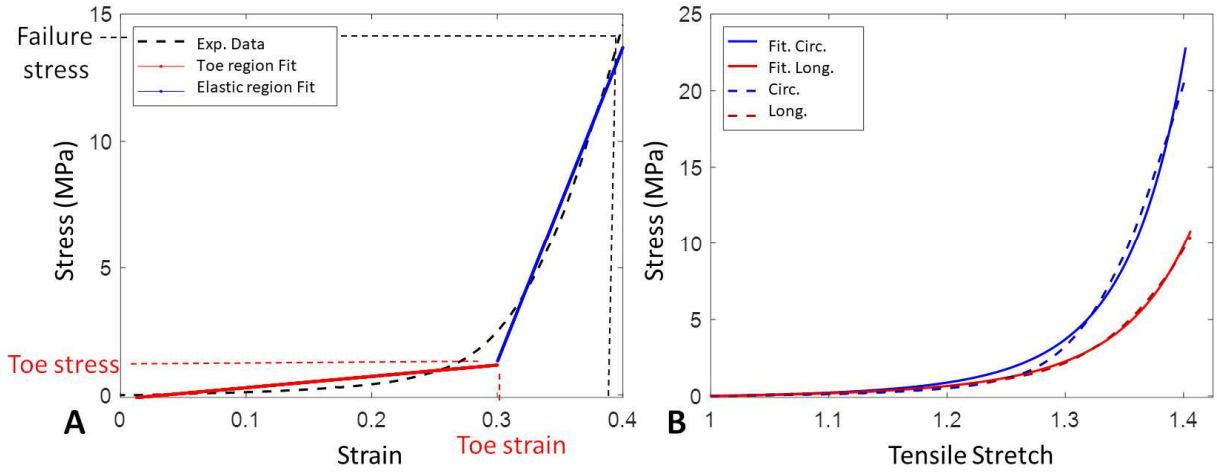

Figure 4 – DAC (A-B) and PM (C-D) biaxial tensile test results according with spinal locations, longitudinal (A-C) and circumferential (B-D).

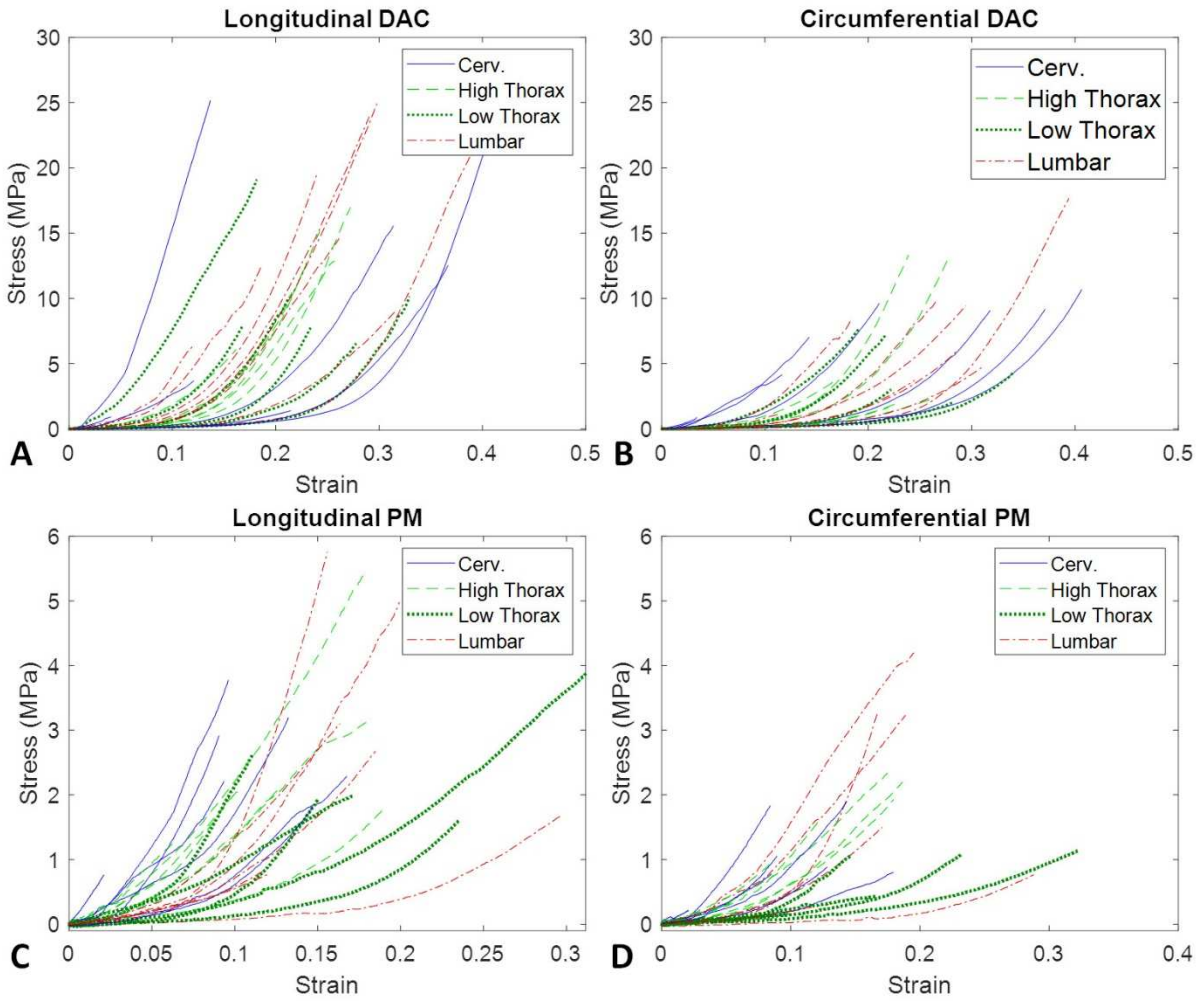

Figure 5– Collagen fibers at different spinal locations of DAC (cervical anterior A and posterior B, high thoracic anterior C and posterior D, low thoracic E, and lumbar spine F)

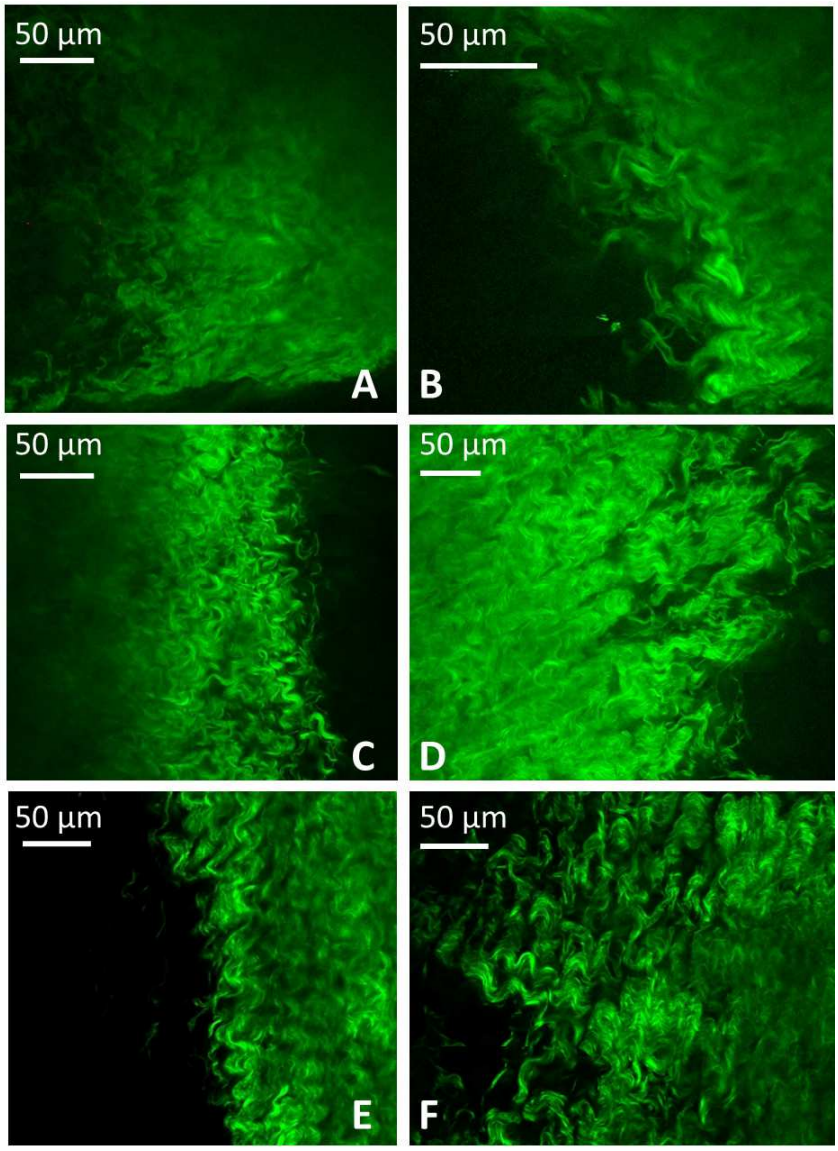

Figure 6 **-** Collagen fibers at different spinal locations of PM (cervical A, thoracic B -C and lumbar spine D, with microscopic visualization of vessel E and F using the Keyence microscope) depicting fenestration within the PM structure.

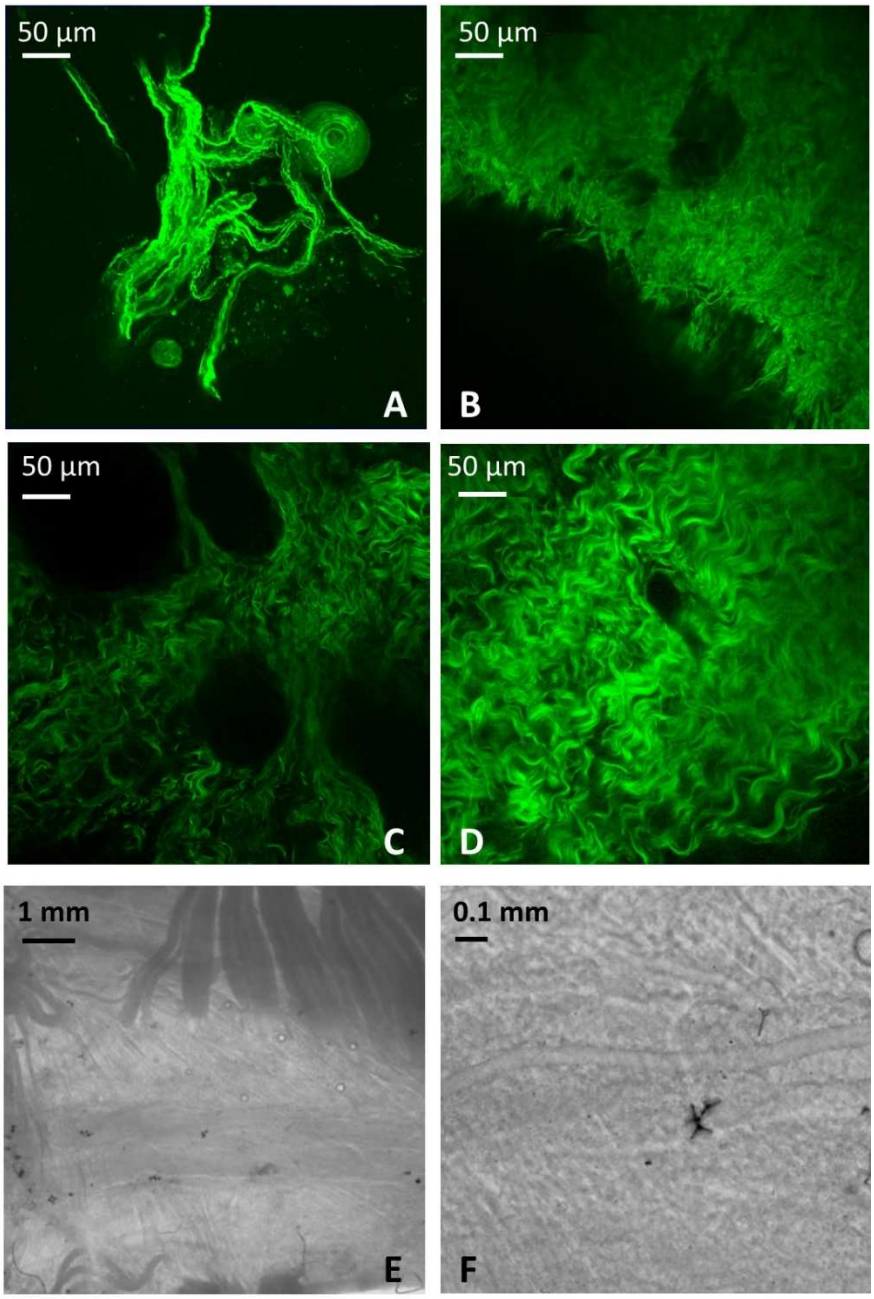

Table 1 – Constitutive models. NH: Neo-Hookean, see Method section for strain energy function's parameter definition. Rad: radiant

Name	**Nb of par.**	**Parameters**	**Model used for the matrix-based material W_{matrix}, number of fibers population**	**Ref.**	**Strain Energy function**
Ogden	2	**μ**(MPa) **β** (-)	isotropic modified Ogden model (n=1)	[38]	$W_{fibres} = \frac{\mu}{\beta^2}[\lambda_{11}^{\beta} + \lambda_{22}^{\beta} + \lambda_{33}^{\beta} - 3]$
Reduced GOH	3	C_{10}(MPa) k_1(MPa) k_2(-)	matrix based NH model, and κ=1/3 (maximum dispersion), 1 fibers population	[32]	$W_{red\_GOH} = C_{10}(I_1 - 3) + \frac{k_1}{2k_2}[e^{k_2\{kI_1-1\}^2} - 1]$
Ani. GOH	5	C_{10}(MPa) k_1(MPa) k_2(-) **κ** (-) **β** (rad)	matrix based NH model, 1 fibers population	[32]	$W_{Ani.GOH} = C_{10}(I_1 - 3) + \frac{k_1}{2k_2}[e^{k_2\{\kappa I_1+(1-3\kappa)I_4-1\}^2} - 1 + e^{k_2\{\kappa I_1+(1-3\kappa)I_6-1\}^2} - 1]$
Trans. Iso Gasser	6	C_{10} (MPa) C_{20}(MPa) k_1(MPa) k_2(-) **κ** (-) **β** (rad)	matrix based Yeoh model, 1 fibers population	[14]	$W_{TIG} = C_{10}(I_1 - 3) + C_{20}(I_1 - 3)^2 + \sum_{i=4,6}\frac{k_1}{2k_2}[e^{k_2\{k(I_1-3)+(I_1-3k)(I_i-1)\}^2} - 1]$
Ani. Gasser	10	C_{10} (MPa) C_{20}(MPa) k_1(MPa) k_2(-) **κ** $_1$(-) **β** (rad) k_3(MPa) k_4(-) **κ** $_2$ (-) **γ** (rad)	matrix based Yeoh model, 2 fibers populations	[14]	$W_{Ani.Gasser} = C_{10}(I_1 - 3) + C_{20}(I_1 - 3)^2 + \frac{k_1}{2k_2}[e^{k_2\{\kappa_1(I_1-3)+(I_1-3\kappa_1)(I_4-1)\}^2} - 1] + \frac{k_3}{2k_4}[e^{k_4\{\kappa_2(I_1-3)+(1-3\kappa_2)(I_6-1)\}^2} - 1]$
Mooney-Rivlin Fibers strengthening	6	C_{10}(MPa) C_{30}(MPa) k_1(MPa) k_2(-) **κ** (-) **β** (rad)		[38]	For $\lambda_d \leq 1$, $W_2 = 0$ For $1 < \lambda_d \leq \lambda_d^*$, $W_{21} = k_3\left(e^{-k_4(\lambda_d-1)} - 1\right)$ For $\lambda_d^* < \lambda_d$, $W_{22} = k_1\lambda_d + k_2$.

Table 2 – DAC biaxial tensile test results and constitutive model parameters. Values depict average of all DAC samples and constitutive models were fitted on each experimental couple of curves before being averaged. Rad: radiant.

DAC	**Parameters**						r^2 (-)	**RMSE** (MPa)
Bi-linear	**E**(MPa)	**Toe strain**(-)	**Toe stress**(MPa)	**Failure strain** (-)	**Failure stress** (MPa)			
Long	108.1±40.3	0.13±0.08	1.60±0.81	0.239±0.086	13.85±7.03		0.980±0.001	
Circ	53.2±31.70	0.14±0.08	1.06±0.83	0.240±0.087	6.78±6.10		0.979±0.002	
Ogden	**μ**(MPa)	**β** (-)						
	2.83±3.95	0.75±0.20					0.754±0.202	2.216±1.777
Reduced GOH	C_{10}(MPa)		k_1(MPa)	k_2(-)				
	0.478±1.005		53. 67±62.19	48.59±177.58			0.754±0.202	2.215±1.781
Ani. GOH	C_{10}(MPa)		k_1(MPa)	k_2(-)	**κ** (-)	**β** (rad)		
	0.03±0.11		18.36±21.63	42.95±177.87	0.19±0.12	0.76±0.67	0.992±0.005	0.44±0.30
Trans. Iso Gasser	C_{10} (MPa)	C_{20}(MPa)	k_1(MPa)	k_2(-)	**κ**(-)	**β** (rad)		
	0.04±0.15	1.73±2.57	12.23±19.56	41.10±178.13	0.13±0.14	0.76±0.71	0.993±0.004	0.43±0.30
Ani. Gasser	C_{10}(MPa)	C_{20}(MPa)	k_1(MPa)	k_2 (-)	κ_1 (-)	**β** (rad)		
	0.02±0.08	1.62±2.95	7.50±13.34	18.82±45.14	0.23±0.13	0.87±0.74	0.99±0.02	0.27±0.21
			k_1 (MPa)	k_4 (-)	κ_2 (-)	**γ** (rad)		
			3.53±7.87	11.95±20.74	0.06±0.09	0.03±0.12		

Table 3 **–** PM biaxial tensile test results and constitutive model parameters. Values depict average on all PM samples and constitutive models were fitted on each experimental couple of curves before being averaged. Rad: radiant.

Pia Mater	**Parameters**						r^2 (-)	**RMSE** (MPa)
Bi-linear	**E** (MPa)	**Toe strain**(-)	**Toe stress**(MPa)	**Failure strain**(-)	**Failure stress**(MPa)			
Long	26.3±13.3	0.056±0.049	0.29±0.207	0.150±0.065	2.56±1.33		0.980±0.003	
Circ	12.9±8.7	0.054±0.053	0.16±0.128	0.148±0.068	1.36±1.03		0.980±0.003	
Ogden	**μ**(MPa)	**β** (-)						
	1.86±1.48	0.71±0.27					0.75±0.23	0.41±0.28
Mooney-Rivlin	C_{10}(MPa)	C_{30}(MPa)						
	-4.18±4.53	4.35±4.07					0.71±0.28	0.43±0.3
Reduced GOH	C_{10}(MPa)		k_1(MPa)	k_2 (-)				
	0.45±0.41		40.57±53.49	23.52±44.25			0.43±0.31	0.43±0.31
Ani. GOH	C_{10}(MPa)		k_1(MPa)	k_2 (-)	**κ** (-)	**β** (rad)		
	0.09±0.18		12.73±16.74	28.84±47.28	0.22±0.08	0.96±0.6	0.995±0.004	0.069±0.057
Trans. Iso Gasser	C_{10}(MPa)	C_{20}(MPa)	k_1(MPa)	k_2 (-)	**κ** (-)	**β** (rad)		
	0.10±0.19	0.71±1.09	9.44±17.50	22±45.71	0.14±0.12	0.90±0.62	0.995±0.004	0.066±0.056
Ani. Gasser	C_{10}(MPa)	C_{20}(MPa)	k_1(MPa)	k_2 (-)	κ_1 (-)	**β** (rad)		
	0.06±0.12	0.76±1.64	7.76±13.55	25.82±85.53	0.211±0.097	0.80±0.68	0.996±0.004	0.059±0.050
			K_3 (MPa)	k_4 (-)	κ_2 (-)	**γ** (rad)		
			2.39±4.40	16.73±24.93	0.069±0.097	0.05±0.14		
Fibers strengthening	C_{10}(MPa)	C_{30}(MPa)	k_1 (MPa)	k_2 (-)	k_3 (-)	**β** (rad)		
Mooney-Rivlin	0.05±0.22	1.70±0.59	4.67±3.88	32.93±17.70	44.77±12.68	0.80±0.08	0.84±0.10	0.37±0.23

Table 4 – Biaxial tensile test results according with sample spinal locations: Mean±standard deviation (mixed effect standard error). $ depict significant difference assessed by Wilcoxon test between the two locations ($0.01<p<0.05$: $^{\$}$, $0.001<p<0.01$: $^{\$\$}$, $p<0.001$: $^{\$\$\$}$) and * the significant difference assessed by Wilcox test between circumferential and longitudinal direction ($0.01<p<0.05$: *, $0.001<p<0.01$: **, $p<0.001$: ***).

			n	E (MPa)	Toe strain (n.a)	Toe stress (MPa)	Failure strain (n.a)	Failure stress (MPa)
Long	*DAC*	*Cervical*	*8*	106.5±67.6 (27.9)	0.11±0.11	1.4±1.14	0.24±0.13	15.16±10.59
		High Thorax	*8*	122.5±30.2 (27.7)**	0.14±0.05	1.94±0.73	0.25±0.06	15.65±5.47**$^{\$}$
		Low Thorax	*10*	98.8±17.1 (8)***	0.14±0.08	1.57±0.67*	0.23±0.07	10.64±4.10**$^{\$}$
		Lumbar	*5*	96.8±27.5 (20.1)**	0.11±0.05	1.28±0.46	0.23±0.08	13.29±6.74
	PM	*Cervical*	*7*	31.9±10.7 (9.4)**	0.03±0.03	0.22±0.28	0.11±0.05$^{\$1\$2}$	2.42±0.99*
		High Thorax	*9*	27.2±17.1 (12.7)*	0.04±0.04	0.3±0.22	0.13±0.04	2.72±1.75
		Low Thorax	*5*	22.9±10.7 (8.7)*	0.09±0.06	0.37±0.16	0.20±0.08$^{\$2}$	2.41±0.90**
		Lumbar	*5*	20.2±10.9 (10.4)	0.08±0.06	0.27±0.10	0.19±0.07$^{\$1}$	2.64±1.59
Circ	*DAC*	*Cervical*	*8*	58.5±31.2 (26.9)	0.13±0.13	1.09±1.17	0.24±0.13	9.10±9.56
		High Thorax	*8*	58.6±44.6 (32)	0.16±0.05	1.29±0.99	0.25±0.06	7.05±5.79
		Low Thorax	*10*	44.3±17.2 (10.1)	0.15±0.07	0.92±0.24	0.23±0.07	4.63±2.61
		Lumbar	*5*	48.3±22.6 (19.4)	0.13±0.07	0.77±0.39	0.23±0.08	5.98±3.30
	PM	*Cervical*	*7*	14±6.6 (4.7)	0.04±0.03	0.13±0.10	0.10±0.05$^{\$1\$2}$	1.07±0.60
		High Thorax	*9*	15.6±10.9 (8.1)$^{\$}$	0.04±0.03	0.2±0.16	0.13±0.05	1.56±0.98
		Low Thorax	*5*	6.7±4.9 (5.7)$^{\$}$	0.09±0.08	0.16±0.15	0.19±0.09$^{\$2}$	0.78±0.45
		Lumbar	*5*	12.9±8.7 (6.9)	0.06±0.07	0.11±0.06	0.19±0.06$^{\$1}$	1.99±1.67

Table 5 – Fibers characteristics measured using the bi-photon microscopy for DAC and PM samples. The sinusoidal geometrical description of the selected fiber is described by the angle of a direct line through the fiber, Amp is the amplitude of the sinusoidal signal, 1/2P is the half period and fiber thickness is a thickness measured perpendicular to the sinusoidal signal. The fiber volume fraction is defined by thresholding grey level of the whole acquired two-photon images. Rad: radiant.

		Angle (rad)	**Amp** (µm)	**1/2 P** (µm)	**Fiber thickness** (µm)	**Fiber volume fraction** (%)
DAC	Cervical	3.59 (2.88-4.13)	5.1 (4.1-6.7)	9.1 (8.1-10.6)	4.6 (3.5-6.3)	19.8
	Thorax	3.2 (2.55-4.28)	8.3 (7.5-9.2)	32.8 (28.1-37.0)	16.4 (14.6-17.5)	23.4
	Lumbar	3.71 (3.18-4.47)	4.9 (4.3-5.8)	23.6 (20.7-3)	12.5 (10.4-15.5)	34.6
PM	Cervical	2.43 (1.30-3.2)			7.7 (4.9-11.6)	17.3
	Thorax	1.10 (0.97-1.27)	5.3 (3.2-9.3)	20.1 (7.6-27.6)	6.2 (5.9-6.5)	25.4
	Lumbar	2.28 (1.42-3.43)	7.0 (6.7-7.4)	37.7 (32.7-41.5)	13.5 (10.6-16.5)	22.7

Two-photon microscopy

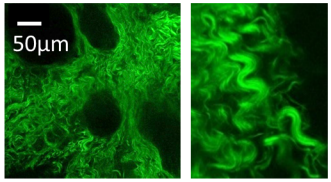

Biaxial Tensile Test

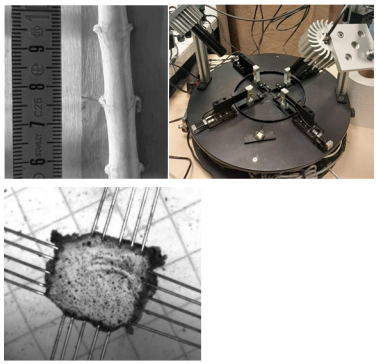

Dura and Arachnoid Complex (DAC)

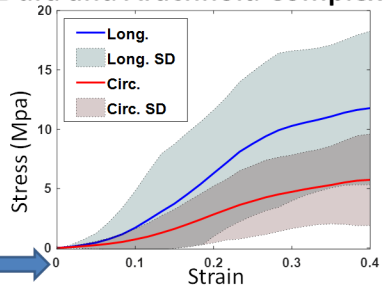

Pia Mater (PM)

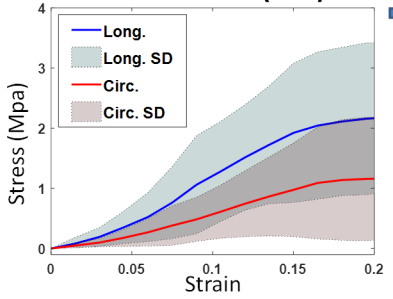

DAC

Anisotropic Gasser

$$W_{\text{Ani. Gasser}} = W_{\text{matrix}} + \frac{k_1}{2k_2}\left[e^{k_2\{\kappa_1(I_1-3)+(I_1-3\kappa_1)(I_4-1)\}^2} - 1\right] + \frac{k_3}{2k_4}\left[e^{k_4\{\kappa_2(I_1-3)+(1-3\kappa_2)(I_6-1)\}^2} - 1\right]$$

PM

Transversely isotropic Gasser

$$W_{\text{Trans. Iso Gasser}} = C_{10}(I_1-3) + C_{20}(I_1-3)^2 + \sum_{i=4,6}\frac{k_1}{2k_2}\left[e^{k_2\{k(I_1-3)+(I_1-3k)(I_i-1)\}^2} - 1\right]$$